GA–A26566

DEPENDENCE OF RESONANT MAGNETIC PERTURBATION EXPERIMENTS ON THE DIII-D PLASMA SHAPE

by
B. HUDSON, T.E. EVANS, C.C. PETTY
and P.B. SNYDER

OCTOBER 2009

GENERAL ATOMICS

DISCLAIMER

GA–A26566

DEPENDENCE OF RESONANT MAGNETIC PERTURBATION EXPERIMENTS ON THE DIII-D PLASMA SHAPE

by
B. HUDSON,* T.E. EVANS, C.C. PETTY
and P.B. SNYDER

This is a preprint of a paper to be presented at the 12th International Workshop on H-mode Physics and Transport Barriers, September 30–October 2, 2009 in Princeton, New Jersey and to be published in Nucl. Fusion.

*Oak Ridge Institute for Science Education, Oak Ridge, Tennessee

Work supported in part by
the U.S. Department of Energy under
DE-FC02-04ER54698, DE-AC05-06OR23100
and DE-FG02-95ER54309

GENERAL ATOMICS PROJECT 30200
OCTOBER 2009

ABSTRACT

The shape of the cross-section of fusion plasma experiments in many devices is a key determinant of the resulting plasma characteristics. Experiments to attempt suppression of ELMs by the technique of Resonant Magnetic Perturbation were performed in the DIII-D tokamak in varying plasma shapes. It was found that while ELM suppression in a plasma shape similar to the ITER shape with a single magnetic null was possible, ELM suppression could not be attained in a balanced or upward-biased double-null shape, although the ELMs in the double-null shape were smaller and higher frequency than the ones before RMP was applied. Calculation of the peeling-ballooning stability of the plasma found that the ELMing plasma is stable to Type I ELMs, suggesting the ELMs are of another type. The magnetic island overlap in the plasma edge is reduced in the double-null shape due to larger separation of resonant surfaces.

1. INTRODUCTION

One of the key concerns in making the ITER project successful is the mitigation of edge localized modes (ELMs) [1], which are transient instabilities typically driven by pressure or current gradients in the edge pedestal region of H-mode [2] plasmas. ELMs result in large transient heat flux that, when scaled to ITER dimensions, are expected to be sufficient to cause physical damage to the diverter target plates or other plasma-facing components. In DIII-D, a number of techniques to suppress ELMs are being studied, such as "QH-mode" [3], where instead of ELMs, the plasma exhibits a high frequency oscillation of low n magnetic modes near the plasma edge. There is also the "ELM-free H-mode" [4] that has no ELMs across the L-H transition and for some time thereafter, until the pedestal pressure gradient builds up to a point sufficient to trigger an "X-event" instability [5,6]. Finally, the technique of resonant magnetic perturbation (RMP) [7–13] has successfully suppressed ELMs in some conditions in DIII-D, where a resonant $n = 3$ magnetic perturbation is applied through the use of external radial magnetic field coils [14,15]. This is believed to render the edge magnetic topology stochastic, increasing transport and reducing the edge pressure and current gradients to the point where peeling-ballooning (P-B) [6,16] modes, which result in Type I ELMs, are stable and ELMs are suppressed.

ELM suppression has been successfully demonstrated in an ITER similar shape in DIII-D, but not at low collisionality in a double-null (DN) shape in typical of advanced tokamak [17] (AT) scenarios in DIII-D. The DN shape has more balanced X-points, approximately equidistant from the last closed flux surface. This results in a higher shaping factor defined as $q_{95}\,(I_P/aB_T)$. The DN shape, while not the most similar to ITER, is important because it has reached higher beta values than the lower single-null (LSN) shape [18]. Additionally, the gradients in the H-mode pedestal should reach higher values before ELMing in the DN shape; this is understood through P-B theory as the effect of high shaping which increases the available operating range of pressure and current gradients before the onset of Type-I ELMs.

Attempts to obtain RMP ELM suppression in DN plasmas have only been successful when the plasma is biased towards having a dominant lower X-point. In balanced and upward biased DN plasmas, RMP ELM suppression has never been obtained although significant efforts have been made during experiments with density, RMP coil current, toroidal rotation and edge safety factor scans in both low (0.1) and high (1.0) collisionality plasmas [7]. The ITER similar shape (ISS), which we more generally refer to as a LSN shape, has a primary X-point in the lower half of the plasma, with a secondary X-point far above the upper half of the last closed flux surface.

The robustness of the technique of RMP ELM suppression is an issue of some importance as it applies not only to ITER but also to other future machines that need to eliminate large transient heat loads to the divertor. As ELM suppression is believed to be equally important in advanced tokamak scenarios as the conventional H-mode scenario, experiments in DIII-D were performed that attempted to suppress ELMs in the DN shape. Ultimately, though RMP changed the character of the ELMs, they could not be suppressed as in the ISS shape. The reasons for this are not yet understood, but the experimental techniques and results are described in this paper.

Section 2 presents a brief discussion of shape in the context of DIII-D plasmas, the motivations for and effects of different shapes, and the control methods for creating them. Section 3 describes RMP ELM suppression experiments in the DN shape, the various parameters scanned and the results observed. Also presented is a discussion of the ELMs during RMP in the DN shape, contrasting them with the Type I ELMs before RMP. Section 4 examines the results of theoretical stability calculations for an ELMing and ELM-suppressed plasma in the two shapes. The conclusions are given in Section 5.

2. PLASMA SHAPING IN DIII-D

The DIII-D [19] tokamak is a toroidal confinement device, with major radius R = 1.7 m, minor radius a = 0.6 m, toroidal magnetic field B_T = 1.7 T, plasma current I_p = 1.2 MA. For typical H-mode plasmas β_N = 1.0 – 2.0 and q_{95} ranges from 3–6. In DIII-D, the inner wall is composed of carbon tiles in roughly a D-shape and there is a set of 18 poloidal field shaping coils which are up-down symmetric relative to the vessel midplane. The plasmas generated are thus typically D-shaped; however, using poloidal field coils the plasma shape can be varied extensively. There are several parameters used to describe a plasmas shape in macroscopic terms, the three major ones being triangularity δ, elongation κ, and squareness ξ. In DIII-D, experiments have been performed in plasmas that range from the D-shape, with elongations up to 2.2, to nearly a circular shape, with elongations as low as 1.2. It was found that elongated plasmas have increased confinement and higher beta limits. By adding triangularity, higher beta toroidal is obtained, enabling an increased ideal wall beta limit [20,21]. Also, by modifying the shape it is possible to change the shear profiles in the plasma, which are known to affect the level of turbulent-driven transport [22]. Experimentally, in DIII-D the shape is pre-programmed into a plasma control system (PCS) [23], which is a feedback-controlled algorithm that adjusts the poloidal field coils in real-time to maintain the programmed shape.

For many years, the DN shape was the most prevalent in DIII-D research, especially in steady state and advanced tokamak scenarios. Having two balanced nulls results in several important benefits to plasma performance. First, because escaping particles to first order follow the separatrix, the location of the escaping particle flux can be controlled by modifying the magnetic geometry. With two nulls, it is possible to pump in two different locations, in this case at the top and bottom of the machine, and thus maintain better control of the overall particle inventory. Second, the heat flux to the wall could be spread out over two divertors instead of one. There are two strike points associated with each “leg” of an X-point, though the particle loss is mainly on the outer, or low-field side, strike point. Third, the DN shape allows a symmetric variation of ξ, which is known to further increase the beta values reached in DIII-D to well over the no-wall limit approximately to the ideal-wall limit.

For the purposes of this paper, any discussion of shape is limited to the poloidal cross-section; the aspect ratio and non-axisymmetric features are excluded. Also, unless specifically noted, the shape refers to a time during the plasma current flat-top, not during breakdown or current ramp-up or ramp-down.

3. ELM SUPPRESSION EXPERIMENT IN THE BALANCED DOUBLE-NULL SHAPE

The DIII-D experiments analyzed here attempted to demonstrate RMP ELM suppression in a low-torque plasma, one with fewer co-injected neutral beam sources in order to have a relatively low rotation. Typical plasma parameters in this experiment were, I_p = 1.2 MA, B_T = 1.5 T, β_N = 2.5 and $q_{95} \sim 3.6$. On successive shots, a scan of the applied current in the I-coils, which determine the relative resonant perturbation strength, was done. The I-coil current was varied between 0 and 5 kA, the former being a reference case. Even parity of the I-coil was utilized, that is, the top and bottom coil currents were in phase. The density pump-out, which is a ubiquitous feature of RMP, was observed in the DN shape and increased with I-coil current. In the LSN ISS, an empirical window for RMP ELM suppression was observed in q_{95}, the safety factor at the surface within which 95% of the normalized poloidal flux is contained. It is typically in the 3.5–3.7 range, but can vary somewhat depending on the discharge. To scan q_{95} in an effort to find the ELM suppression window in these cases, I_p was ramped at a fixed B_T for each of the I-coil currents. In all cases, the ELMs decreased in amplitude, and increased in frequency, during RMP, but were not suppressed. Moreover, there was no observed change in the ELMs during RMP when q_{95} was being scanned.

In this paper we will examine two discharges, one during the LSN ISS experiment in which ELMs were suppressed and compare it with a discharge with the same B_T, q_{95}, β_N, and a similar I-coil current but in the downward-biased DN plasma shape which did not have complete suppression of ELMs. The flux surfaces of the two shapes are compared in figure 1. We see that the DN shape has two distinct nulls inside the vessel, whereas the ISS has only the lower null inside the vessel. The two flux surfaces shown for each shape denote the primary and secondary separatrices attendant to their respective X-points. The degree to which the plasma is a LSN, balanced, or USN, is determined by the separation of the two flux surfaces at the midplane. This is adjusted with the PCS to control the shape. In figure 1, it can be seen that the more balanced DN shape has a smaller gap between the flux surfaces at the midplane than the ISS. Also, the ISS has a more rounded upper half, and hence less triangular in shape as previously discussed.

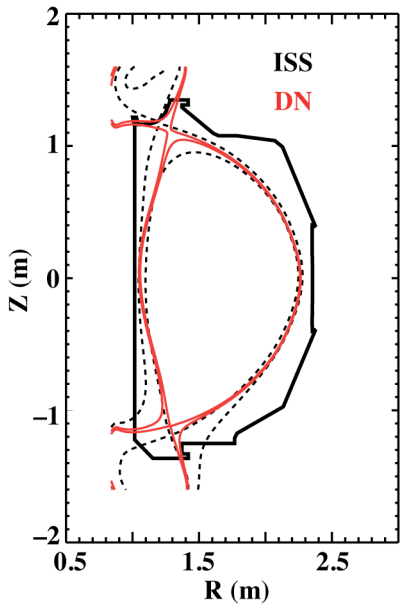

Figure 1. Flux surfaces from equilibrium reconstruction for an ISS (red solid) and a DN shape (black dashed). The upper null in the ISS is calculated to be at or beyond the boundary of the carbon tile wall.

The absence of a window in q_{95} for RMP ELM suppression in the DN shape (#133904), in contrast to the ISS case (#129949), is clearly seen in figure 2. Figure 2(a) shows I_p and the I-coil currents. In the DN shape, I_p was lowered prior to RMP in order to have a higher q_{95}. After 3500 ms, I_p is ramped slowly to scan through q_{95} to attempt to reach the empirical "q_{95} resonance window" and attain ELM suppression. The plasma current in the ISS is terminated by a disruption due to a locked mode. The time traces for q_{95} are shown in figure 2(b). For the ISS, q_{95} is fairly constant at about 3.6, highlighted by the horizontal dashed line, whereas the DN discharge shows the reduction of q_{95} due to the I_p ramp. The times at which the two plasmas have approximately the same relevant parameters are 3100 ms for the ISS and 5400 ms for the DND shape. The ELMs are shown in figure 2(c)(DN) and figure 2(d) (ISS) by bursts of D_α light, collected by an array of filterscopes [24] viewing the lower DIII-D divertor. Emission increases during ELMs due to increases in electron impact-excitation from neutrals released by an increase in plasma-wall interactions. In both discharges, the ELMs before RMP are large, comparatively low-frequency Type I ELMs, typical of high-beta H-mode plasmas. During RMP, the ELMs in the ISS shape are completely suppressed for 900 ms, until shortly before a tearing mode slows down and locks to the wall, terminating the discharge. ELMs in the DN discharge are reduced in size, but still present and at a higher frequency.

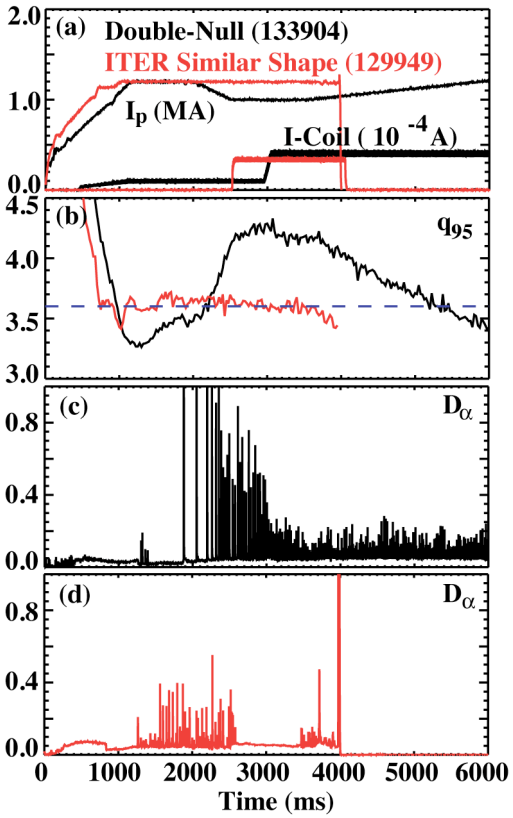

Figure 2. Time traces for the ISS discharge (red) and DN discharge (black). (a) I_p and I-coil currents. I_p is ramped in the DN after 3500 ms to scan q_{95}. (b) q_{95}. The two plasmas have similar q_{95} of 3.6 at 3100 and 5400 ms, respectively. (c) D_α emission. The ISS shaped plasma has a window of complete ELM suppression. ELMs remain during the RMP in the DN shaped plasma, though smaller and more rapid.

An expanded view of the ELM's time history across the I-coil turn-on in the DN shape is shown in figure 3. The lower trace shows the I-coil current is ramped up over 100 ms from 1 kA at 2950 ms to 4 kA at 3050 ms. The upper trace shows the line-averaged electron density. There is no density pump-out or change in the ELMs until the I-coil current reached 2 kA at about 2970 ms. It is observed that the ELM frequency is proportional to the I-coil amplitude, but the decrease in ELM amplitude is proportional to the density. For the small ELMs during RMP, there are what appear to be "grassy" Type II or Type III ELMs, which are clearly not present prior to the I-coil turn-on at 2950 ms or they appear at 3000 ms. The ELM period decreases from about 30 to 12 ms during the I-coil ramp and is constant thereafter, whereas the density pump-out occurs over a much longer timescale.

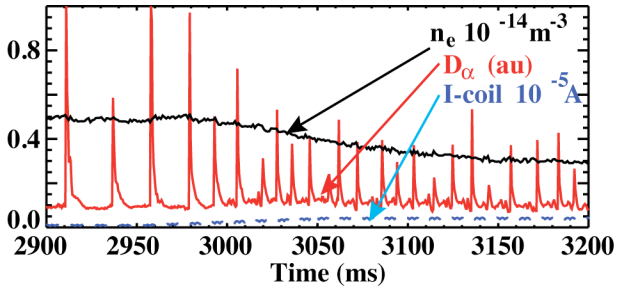

Figure 3. Expanded view of ELMs in the DN shape. The ELMs (red/gray) reduced in size and increase in frequency during the ramp-up of the I-coil current (dashed blue). The size of the ELMs are proportional to the plasma density (black) which also decreases as the I-coil current ramps up. Precursors to the smaller ELMs are observed which are not present prior to the I-coil ramp.

4. PEDESTAL CHARACTERISTICS AND PEELING-BALLOONING STABILITY

The nature of the ELMs during RMP for the DN discharge remains an open question. If these ELMs reside in a stable P-B region then P-B theory would suggest that they are not Type-I ELMs. To calculate the stability of a particular time during a discharge, we must first perform equilibrium reconstruction of the plasma constrained by measurements of the plasma pressure profile in order to obtain the relevant parameters in required for the P-B analysis. The equilibrium reconstruction code EFIT is used, with diagnostic input averaged over a specified time window.

The averaging window taken for equilibrium reconstruction is as long as possible in order to have better statistics for diagnostic constraints on the equilibrium reconstructions. This is subject to the plasma having nearly constant conditions over the averaging time. In the ELMing phases before RMP, the ELMs are sufficiently separated, and we have enough data points that we can use the diagnostic data in the last 20% of the times between ELMs. This allows us to have plasma profiles reflective of the unstable plasma that give rise to the ELMs. In the case of the ISS discharge, averaging was done from 1500 to 2500 ms, before RMP, and from 3000 to 3200 ms during the period of RMP ELM suppression. The number of Thomson scattering measurements used in density and temperature profile averaging in the ISS case was 13 before RMP and 16 during RMP, where every Thomson measurement in the pre-ELM window was used. The DN shape was averaged from 2200 to 2900 ms before RMP and from 5420 to 5500 ms. This resulted in 6 points before RMP and 12 during RMP, where no discrimination in the ELM cycle could be used due to the rapid frequency of the ELMs and the small time window. The averaging window for the DN shape prior to RMP was shorter than in the ISS because the time period between a constant density H-mode and the I-coil turn-on was smaller. For the time during RMP in the DN shape, the averaging window had to be short because q_{95} was varying due to the I_p ramp and we want $q_{95} \sim 3.6$, as it was in the ISS. The smaller number of usable measurements in the DN shape does increase the error in the pressure from about 5% to 10%. The error in the DN during RMP is about 5%, but there is a systematic offset due to the inclusion of all Thomson measurements, instead of the ones just prior to an ELM. In a plasma exhibiting large Type I ELMs, this can impact stability analysis, but the small, frequent and less perturbative ELMs in the DN shape during RMP likely have less impact on the temperature and density profiles.

The gradients of the plasma pressure and current at the edge are believed to drive the instabilities that result in Type I ELMs. The pressure profile is determined experimentally by Thomson scattering [25] (electron), charge-exchange recombination spectroscopy [26] (ion) and a calculation of neutral beam pressure by the ONETWO code [27]. The current profile is calculated by the combination of equilibrium reconstruction with the EFIT code [28] and the Sauter bootstrap current model [29]. The response of the edge parallel electric field to the sudden increase in bootstrap current at the L-H transition ion has been shown to be in agreement with the Sauter model on DIII-D [30]. In these experiments, the edge bootstrap current has no directly measured experimental constraints, therefore we vary the edge current until a minimum-χ^2 solution of the equilibrium basis functions is reached. Figure 4 shows the pressure [figure 4(a)] and current [figure 4(b)] gradients in the pedestal region for the two plasma shapes, both before and during RMP. The ISS (red) has a narrower and lower pedestal than the DN (black). Before RMP, the DN has a slightly larger maximum pressure gradient than the ISS, though they are nearly matched during RMP. The maximum pressure gradient in the ISS is closer to the plasma LCFS, $\psi_N = 1$, than in DN (dashed). The current gradients [figure 4(b)] have the same description as the pressure gradients, as they are strongly constrained to the pressure gradient by the use of the Sauter model, which was scaled less than 20% in each case to reach the minimum-χ^2 fit.

The ELITE [31] code performs P-B stability analysis which is represented as the growth rate of intermediate n modes as a function of the edge pressure and current gradients that are calculated from equilibrium reconstruction. In addition, it is often instructive to see the stability boundary in P' and J' space, as the distance to the boundaries combined with the estimated error in the calculation provide additional insight when comparing different equilibria. The pressure and current gradients are then scaled around the experimental value and the stability is calculated at each point, providing a mapping of the stability contour.

In figure 5, the stability in P' and J' space is shown by a contour where on one side (red), the growth rate of the least-stable mode is positive, indicating instability and negative on the other side (blue), being stable. The contour denotes the critical growth gradients that will result in instability to P-B modes. The stability plots for the ISS [figure 5(a)] and DN shape [figure 5(b)] prior to RMP, show the plasmas in both shapes to be unstable to P-B modes, in particular the current-gradient driven peeling mode. The unstable plasma is expected to exhibit Type I ELMs, which are observed experimentally. Similar analysis is done for the two discharge shapes during which RMP was applied (figure 6), when the relevant physical parameters for ELM suppression were closely matched, but where the DND shape did not show ELM suppression whereas the ISS did. The operating points, denoted by the cross-hairs move to lower P' and J',

as with the decreased gradients shown in figure 4. The ISS, figure 6(a), and the DN shape, figure 6(b), are calculated to be stable to P-B modes, and thus P-B theory suggests that the observed ELMs may be something other than Type I ELMs. Also, as seen in figure 6, the region of stability in the higher triangularity DN shape is expanded from the more rectangular stable space present in the lower triangularity ISS. This expansion of the stability space is one of the main reasons to explore the DN shape when developing AT scenarios.

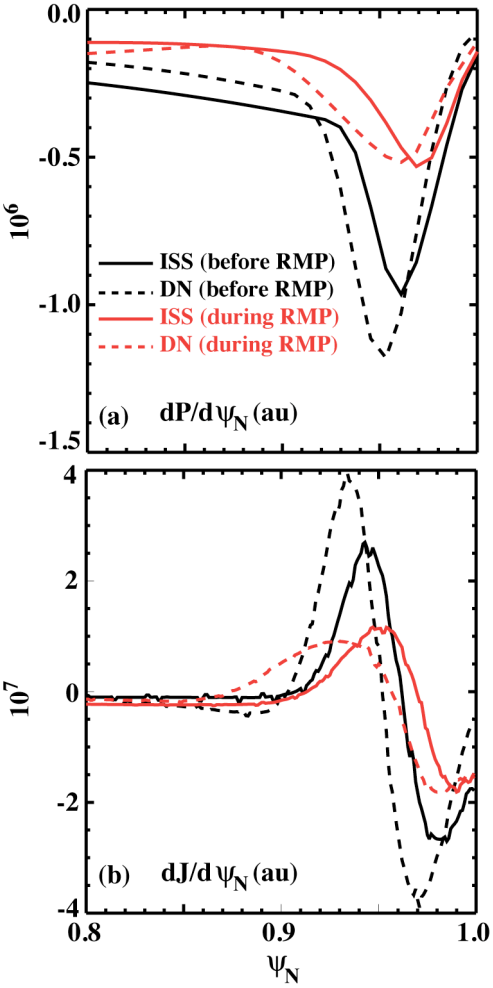

Figure 4. Pressure (a) and current (b) gradients in the pedestal. The times prior to RMP are shown in black; during RMP in red (gray). The solid lines corresponds to the ISS; the dashed lines the DN shape.

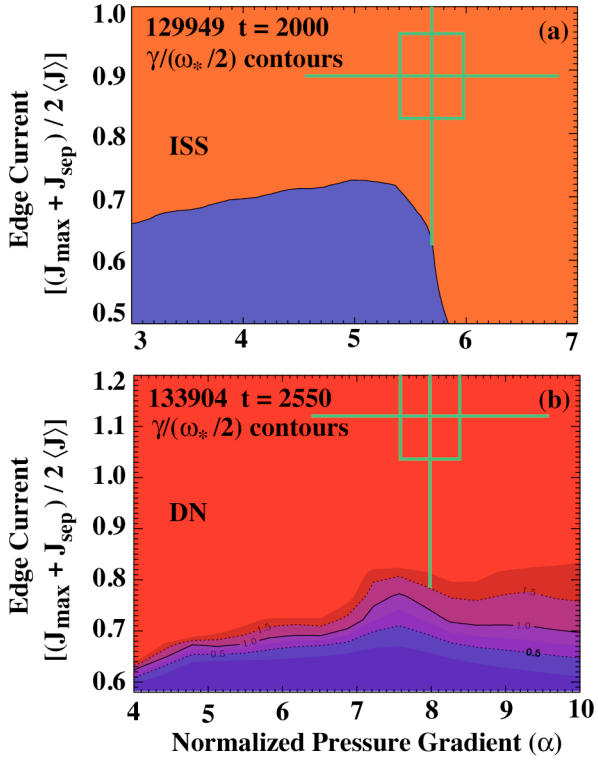

Figure 5. ELITE calculation of P-B stability prior to RMP for (a) the ISS and (b) the DN shape. The red region is stable to P-B modes; the blue is unstable. The operating point is shown by the crosshairs.

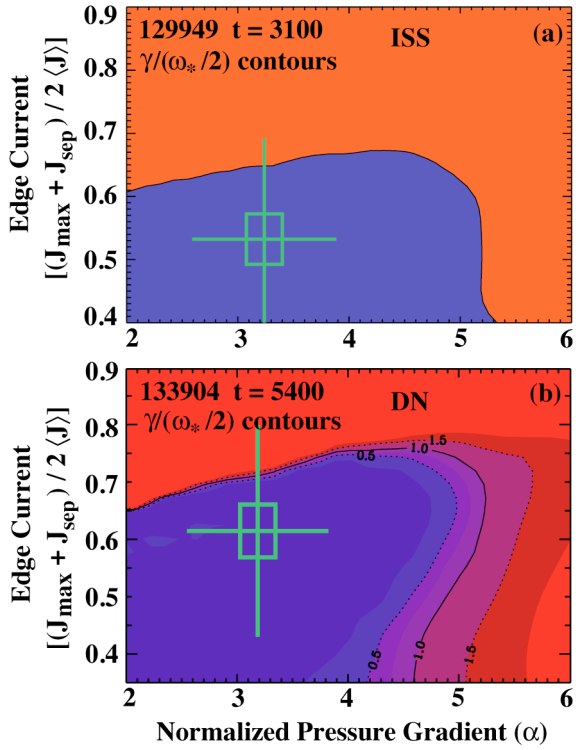

Figure 6. ELITE calculation of P-B stability after to RMP for the (a) ISS and (b) DN shape. The red region is stable to P-B modes; the blue is unstable. The operating point is shown by the crosshairs.

The working explanation of why RMP results in a decrease of the pedestal pressure and current gradients is that the external perturbation leads to large saturated magnetic islands, which in the edge, overlap and become stochastic, thus increasing particle and energy transport. It has been calculated that in high-beta discharges, where the pedestal gradients are comparatively large even during RMP, that the substantial edge bootstrap current introduces a non-negligible distortion of the local q profile away from a simple monotonically increasing function of ψ_N [32]. This distortion typically manifests itself as a flattening of the q-profile in the pedestal region. Quasi-linear island theory [33] states that the magnetic island width scales as $W \propto \sqrt{1/q'}$, with q' being the magnetic shear or the derivative of q with poloidal flux. The other factor affecting island overlap being the distance between resonances. A region of flat q separates resonances, which reduces island overlap. In figure 7 the Chirkov overlap parameter [34],

$$S = \frac{W_i + W_{i-1}}{2\left(\psi_{N,i} - \psi_{N,i-1}\right)} \quad , \tag{1}$$

where W_i is the width of the ith island and $\psi_{N,i}$ is the location of the resonant surface in normalized poloidal flux space, is plotted for (m = 1–12, n = 3) as a function of ψ_N. With S < 1, the islands are not overlapped in this region and thus the criterion for strong stochasticity would not be reached [35]. In both plasma shapes, S decreases outside of $\psi_N = 0.93$. This is due to the spreading of resonances, resulting from the flattening of q between $0.93 < \psi_N < 0.97$, also shown in the plot, which for the DN shape is more pronounced than for the ISS. In figure 7, we see that for the ISS shape $S > 1$ outside $\psi_N = 0.84$, giving a large enough region of island overlap that complete ELM suppression is expected [36]. However for the DN shape $S < 1$ outside of $\psi_N = 0.94$, and thus the island overlap width is only $\Delta\psi_N = 0.08$ which is too narrow for complete ELM suppression. Without the presence of strong stochasticity, the radial transport of heat and particles thought responsible for reducing the edge pressure and current gradients would be greatly reduced, and this reduced efficacy of RMP in the DN shape is likely responsible for the lack of ELM suppression observed in experiment.

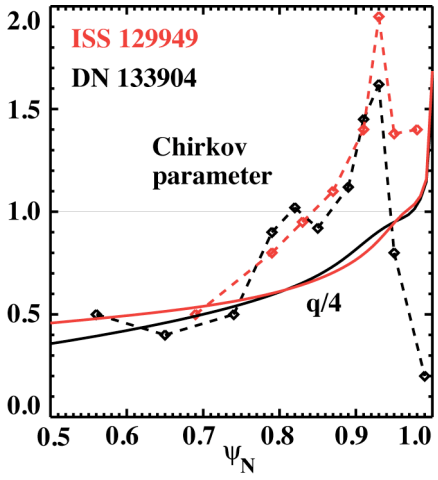

Figure 7. The Chirkov overlap parameter, S, (data points connected with dashed lines) shown for at several $q(m, n=3)$ resonant surfaces and $q\psi_N$ (solid). The ISS is in red (gray) and the DN shape in black.

5. CONCLUSIONS

ELM suppression experiments were attempted in two plasma shapes in DIII-D: the LSN ISS, which is a low-triangularity shape, and a DN shape, which has higher triangularity and two field nulls, approximately equidistant from the equatorial plane. The DN shape is of interest because its higher stability and confinement properties make it a candidate for advanced tokamak scenarios. The DN shape did not show ELM suppression, whereas the ISS did. However, the character of the ELMs changed during application of RMP in the DN shape, becoming smaller, higher frequency and possessing small Type II ELMs between the larger ELMs. Times were selected in the two discharges for detailed analysis when they were matched in terms of electron density, electron temperature, q_{95}, and I-coil current. Computation of P-B stability showed both the ISS and DN plasma shapes to be stable to Type I ELMs during RMP, suggesting that the ELMs observed in the DN shape are not Type I according to P-B theory. Calculation of the Chirkov overlap parameter during RMP revealed that the DN shape had a an edge Chirkov parameter less than one, implying that RMP did not render the edge stochastic, as expected to bring about ELM suppression. The reduction in island overlap was identified as being due to a lower magnetic shear in the edge, due to a large edge current. This contrasted with the ISS shape that had a similar maximum current gradient, but less integrated edge current.

Future work could include experiments where an RMP suppressed lower-biased DN shape is gradually altered to be balanced or upper-biased. If ELM suppression is lost due to the shape change, the pedestal and other plasma parameters, such as the edge magnetic shear, could be studied to find a correlation. Present work is ongoing to add additional RMP coils to the tokamak center-stack, which will allow more control of RMP magnetic configurations and may result in RMP ELM suppression of the balanced or upper-biased DN shape or the USN shape. Future experiments could address also driving resonant perturbations at higher n, possibly making the magnetic field stochastic out to the last closed flux surface. Also, further increasing the I-coil current to overcome the separated resonances in due to a large edge current should be explored.

REFERENCES

[1] H. Zohm, Plasma Phys. Controlled Fusion **38**, 105 (1996)

[2] R. Aymar, P. Barabaschi, and Y. Shimomura, Plasma Phys. Controlled Fusion **44**, 519 (2002)

[3] K. H. Burrell *et al.*, Plasma Phys. Control. Fusion **44,** A253–A263 (2002)

[4] G. Wang *et al.*, J. Nucl. Mater. **363–365**, 534–538 (2007)

[5] J. W. Connor *et al.*, Phys. Plasmas **5**, 2687 (1998)

[6] P. B. Snyder, H. R. Wilson, J. R. Ferron, L. L. Lao, A. W. Leonard, T. H. Osborne, A. D. Turnbull, D. Mossessian, M. Murakami and X. Q. Xu, Phys. Plasmas **9**, 2037 (2002)

[7] T. E. Evans *et al.*, Phys. Rev. Lett. **92**, 235003 (2004)

[8] K. H. Burrell *et al.*, Plasma Phys. Control. Fusion **47**, B37 (2005)

[9] T. E. Evans *et al.*, Nucl. Fusion **45**, 595–607 (2005)

[10] R. A. Moyer *et al.*, Phys. Plasmas **12**, 056119 (2005)

[11] T. E. Evans *et al.*, Phys. Plasmas **13**, 056121 (2006)

[12] T. E. Evans *et al.*, Nucl. Fusion **48**, 024002 (2008)

[13] M. E. Fenstermacher, T. E. Evans, T. H. Osborne, M. J. Schaffer, J. S. deGrassie, P. Gohil, R. A. Moyer and the DIII-D Team, Nucl. Fusion **48**, 122001 (2008)

[14] G. L. Jackson *et al.*, Proc. 30th EPS Conf. on Controlled Fusion and Plasma Physics (St. Petersburg, 2003) CD-ROM P-4.47

[15] T. E. Evans, R. A. Moyer J. Nucl. Mater. **313–316**,1282 (2003)

[16] J. W. Connor *et al.*, Phys. Plasmas **5**, 2687 (1998)

[17] T. S. Taylor, Plasma Phys. Controlled Fusion **39**, B47 (1997)

[18] C. T. Holcomb, Invited APS-DPP Oral Presentation (2008)

[19] J. L. Luxon, Nucl. Fusion **42**, 614–633 (2002)

[20] Y. R. Lin-Liu *et al.*, Phys. Plasmas **6**, 3934 (1999)

[21] J. R. Ferron *et al.*, Phys. Plasmas **12**, 056126 (2005)

[22] L. Lao *et al.*, Nucl. Fusion **39**, 1785 (1999)

[23] P. Gohil *et al.*, Plasma Phys. Control. Fusion 48, A45–A53 (2006)

[24] N. H. Brooks, R. J. Colchin, D. T. Fehling, D. L. Hillis, Y. Mu and E. Unterberg, Rev. Sci. Instrum. **79**, 10F330 (2008)

[25] T. Carlstrom *et al.*, Rev. Sci. Instrum. **63**, 4901 (1992)

[26] P. Raymond *et al.*, Rev. Sci. Instrum. **57**, 2012 (1986)

[27] H. St. John *et al.*, Proc. Fifteenth Intl. Conf. on Plasma Physics and Cont. Nuclear Fusion Research, IAEA, Seville, 26 Sept. **3**, 603 (1994

[28] L. L. Lao *et al.*, Nucl. Fusion **30**, 1035 (1990)

[29] O. Sauter, C. Angioni, and Y. R. Lin-Liu, Phys. Plasmas **6**, 2834 (1999); Phys. Plasmas **9**, 5140 (2002)

[30] M. R. Wade, M. Murakami and P. A. Politzer, Phys. Rev. Lett. **92**, 235005 (2004).

[31] H. R. Wilson, P. B. Snyder, G. T. A. Huysmans and R. L. Miller, Phys. Plasmas **9**, 2377 (2002)

[32] B. F. Hudson *et al.*, to be submitted to Nucl. Fusion (2009)

[33] S. V. Mirnov and I. B. Semenov, At. Energy, **30**, 14 (1971)

[34] B. V. Chirikov, Phys. Rep., **52**, 263 (1979)

[35] J. B. Taylor, Rev. Mod. Phys. **58**, 741 (1986)

[36] M. E. Fenstermacher *et al.*, Phys. Plasmas **15**, 056122 (2008)

ACKNOWLEDGMENT

This work was supported by the US Department of Energy under DE-FC02-04ER54698, DE-AC05-06OR23100 and DE-FG02-95ER54309. The author would like to thank J. Ferron and T. Osborne for helpful discussion.